Rock Mechanics and Rock Engineering (2019) 52:3999–4016
https://doi.org/10.1007/s00603-019-01809-5

ORIGINAL PAPER

Gravitational Search Algorithm for Microseismic Source Location in Tunneling: Performance Analysis and Engineering Case Study

Chunchi Ma[1] · **Yupeng Jiang**[2] · **Tianbin Li**[1]

Received: 4 September 2018 / Accepted: 30 March 2019 / Published online: 25 April 2019

Abstract
Microseismic source location (MSL) provides crucial information for the interpretation of rock mass stability and early warning of rock mass hazards. The accuracy of MSL mainly depends on the formation of the sensor array, the multi-velocity model, and the locating algorithm. Especially, the choice of algorithm plays a decisive role, which requires both optimal accuracy and efficiency for searching the global optimal solution. In this paper, an advanced heuristic algorithm, Gravitational Search Algorithm (GSA), is applied for MSL in tunnel engineering. A standard framework of the GSA-based searching process is first built. Its accuracy, stability, and speed of convergence are rigorously compared and analyzed with particle swarm optimization and simplex algorithm using synthetic and real microseismic data. Four types of equivalent velocity models are combined with the searching algorithm to further discuss the applicability and performance of GSA in different situations. The studies show that for all the cases, GSA has the highest speed of convergence with the best accuracy. Locating errors are controlled within 10 m, which fulfills the requirement of engineering accuracy. A representative case study is conducted using microseismic data prior to a major rockburst in a twin-tube highway tunnel. The calculated cluster of seismic events using GSA-based algorithm well matches the actual unstable areas. This work indicates that GSA is an optimal algorithm for microseismic source location and rockburst warning in tunneling.

Keywords Microseismic source location · Gravitational search algorithm · Velocity models · Rockburst warning · Tunnel engineering

List of symbols

MSL	Microseismic source location
GSA	Gravitational search algorithm
SA	Simplex algorithm
GA	Genetic algorithm
PSO	Particle swarm optimization
G	Gravitational constant
fit	Fitness function of MSL
R_{ij}	Euclidian distance between agent i and j
V	Equivalent velocity at the path of an MS signal
t_i	Observed arrival (trigger) time at the ith sensor
$\boldsymbol{M}$	Set of agents' masses in solution space
$\boldsymbol{X}_i$	Set of ith agent's solution values
F_i^d	Resultant force at dth dimension for the ith agent
a_i^d	Acceleration at dth dimension for the ith agent
v_i^d	Velocity at dth dimension for the ith agent
x_i^d	Position at dth dimension for the ith agent

1 Introduction

Microseismic (MS) monitoring is the foundation of rock mass stability monitoring and rockburst warning in underground engineering. It is widely used in modern tunnel engineering and mine industry to identify the high-risk areas (Feng et al. 2013). The technology involves two main procedures: recording the microseismic signals that released from cracking or deformation events in the surrounding rock mass; tracing back the microseismic source location (MSL) in the three-dimensional space; and extracting seismic properties (e.g., seismic moment, magnitude and apparent stress, etc.). The MSL provides essential information for the MS

✉ Yupeng Jiang
yupeng.jiang@sydney.edu.au

Chunchi Ma
machunchi17@cdut.edu.cn

[1] State Key Laboratory of Geo-Hazard Prevention and Geo-Environment Protection, Chengdu University of Technology, Chengdu 610059, China

[2] School of Civil Engineering, University of Sydney, Sydney, NSW 2006, Australia

monitoring. It could locate the real position of the cracking event cluster, which precisely portraits the distribution and formation of the fracture network in surrounding rocks. Further inversion and forward modeling based on an accurate network model could reveal the evolutionary pattern of rock stability. The early warning of the rockburst during the engineering process can be achieved to ensure the safety (Ma et al. 2016, 2018).

However, problems still lie in the theoretical bases of MSL, especially when the drill-and-blasting method is applied for the tunnel excavation. Such engineering activity inevitably induces strong dynamic disturbances and generates a large amount of MS events around the tunnel face. Unlike traditional MS monitoring in industries of coal mining, oil and coal seam gas exploration (Grigoli et al. 2013; King and Talebi 2007; Gong et al. 2012; Zhang et al. 2015), the spatial distribution of the MS detector array in the tunnel cannot fully cover the MS space due to a highly limited underground space. Hence, the accuracy of the MSL is compromised or even unreliable. Meanwhile, the propagation of MS wave could be strongly affected by the excavated areas of the tunnel, which physically represents a void area that may distort and delay MS signals. High-frequency components of a signal might be deflected and attenuated by the tunnel wall. Fracture zones and other geological structures introduce the heterogeneity and anisotropy into the wave velocity. In such situations, the basic assumption of constant velocity model, which widely applied for MSL methods, is no longer unacceptable. Other factors such as environmental noises could also reduce the quality of signals. Therefore, it is imperative to develop an advanced locating method which has the optimal searching ability and computational efficiency and can also incorporate a multi-velocity model.

Certain progress has been made by some studies. For example, ISRM (Xiao et al. 2015) suggested an improved formation of the sensor array for drill-and-blast and TBM methods in a single tunnel. However, this improvement is still limited by features of the ill-covered array. Heuristic algorithms (Tang et al. 1996; Vandenbergh and Engelbrecht 2006; Rashedi et al. 2009; Farmer et al. 1986; Dorigo et al. 1996; Jiang and Xing 2016; Gazi and Passino 2004) have also been used for calculating the locations of MS events and their equivalent velocities. This kind of algorithms is particularly powerful for solving high-dimensional optimization problems (i.e., MSL with multiple variables). A more realistic velocity model in MSL inevitably introduces extra variables into the searching process. The application of heuristic algorithms has been studied with few classic methods such as the genetic algorithm (GA) (Jones and Rayne 1994; Li et al. 2017), simulated annealing (SA) (Pei et al. 2009), and particle swarm optimization (PSO) (Feng et al. 2015). Their procedures at each iteration step can be summarized into three parts: (i) self-adaption, where agents update their positions towards the global optimal solution; (ii) cooperation, which allows agents to communicate and exchange information with each other; and (iii) competition, which chooses the optimal solution at the current step and examines the convergence. Although heuristic algorithms are sharing a similar framework, each method possesses its unique advantages. It requires researchers and engineers to find the superior method for different situations. SA (Wang et al. 2017; Li et al. 2003) can guarantee a convergence at each iteration step, but has a slow speed for searching the optimal solution. PSO (Chen et al. 2009; Lagos and Velis 2018; Yang et al. 2015) has higher speed of convergence; however, it is relatively easier to be trapped by local minimum values due to the lack of interaction between searching agents. It makes this method less suitable for the problem that has a high-dimensional solution space. GA (Gong et al. 2011; Yuan and Li 2017) generally has a lower efficiency compared with other heuristic algorithms and does not guarantee a global optimal solution after a considerable computational time. However, there is no focused study that addresses this key issue and provides a comprehensive comparison for those algorithms. Therefore, it is very meaningful to study the performance and applicability of existing algorithms. Furthermore, advanced heuristic algorithms should be applied to MSL-related problems and combine it with suitable velocity models to achieve an even better result. For example, Feng et al. (2015) introduced a sectional velocity model into the PSO-based MSL algorithm. They received a significantly better result compared with traditional iterative/non-iterative methods.

In the work, we introduced an advanced heuristic method, gravitation search algorithm (Rashedi et al. 2009) (GSA), to solve MSL problems in deep-buried tunnel engineering with improved velocity models. Its optimization strategy is based on Newtonian gravitational law and the updating strategy is using second Newtonian law. Studies indicate that compared with existing methods, this algorithm is particularly powerful at the second procedure 'communication' and, therefore, shows superiority in both accuracy and efficiency. The basic methodology and framework for GSA–MSL are introduced in Sect. 2. A detailed discussion about its advantages and limitations compared with other MSL methods are also provided. In Sect. 3, the performance of GSA is carefully compared and analyzed with classic MSL methods. A serial of algorithm tests is conducted with both synthetic and real data. Improved velocity models for the twin-tube tunnel are proposed and applied for the tests. Eventually, in Sect. 4, a representative case study of pre-burst MSL that recorded at the MICANG Mountain tunnel is conducted to further demonstrate the application GSA–MSL for early warning of the rockburst. Main findings and general conclusions are presented in the last section.

2 GSA Algorithm for Microseismic Source Location

2.1 Introduction of GSA Algorithm

The searching strategy of GSA is built based on the Newtonian gravitational law, which is written as

$$F = G\frac{M1M2}{R^2}, \tag{1}$$

where M_1 and M_2 are the mass of two agents or, in a solution space, two solutions; R and G denote the Euclidean distance between two agents and the gravitational constant, respectively; and F represents the gravitational force. The mass of an agent is calculated with a target function at each time step as an evaluation of the fitness of a solution (i.e., fitness value). A better solution will be assigned to a larger mass. It can be observed from Fig. 1 that this strategy guarantees a better solution/agent generates a larger attractive force, which attracts other agents move towards its location with a larger acceleration. Meanwhile, this mass also makes the superior agent less movable.

The fitness function is proposed to sum the absolute values of the difference between the observed ($tp,s\ i - t_0$) and calculated arrival time ($R_i/V^{p,s}$) at each sensor. The solution with the smallest difference is the most desirable one for the MSL. The function can be written as

$$fit = \sum_{i=1}^{n}\left|t_i^{p,s} - t_o - \frac{R_i}{V^{p,s}}\right|, \tag{2}$$

where *fit* denotes the fitness value; n is the number of sensors; t_i is the observed arrival time at the ith sensor; t_0 denotes the occurrence time of an MS event; R_i represents the Euclidean distance between the source location and the ith sensor; $V^{p,s}$ is the equivalent velocity of the propagating path of an MS signal; the superscripts p and s denote the compressive and shear wave, respectively. If a fitness value is relatively lower, a larger mass value will be assigned to that agent.

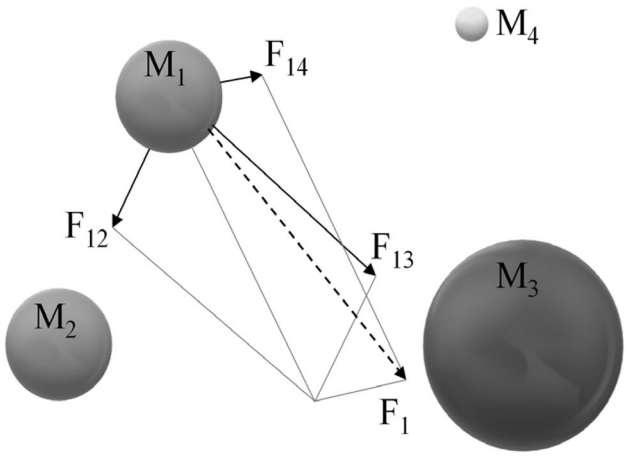

Fig. 1 Schematic diagram of the gravitational interaction between particles (Rashedi et al. 2009)

2.2 Implementation of Microseismic Source Location

a. At the initial step N, number of agents is randomly distributed in the pre-defined solution space; each of the agents has the mass M_i and a solution X_i with n dimensions:

$$M = \left(M_1, \ldots, M_i, \ldots, M_N\right),\ (i = 1, 2, \ldots, N), \tag{3}$$

$$\mathbf{X}_i = \left(x_i^1, \ldots, x_i^d, \ldots, x_i^n\right)^T,\quad (d = 1, 2, \ldots, n), \tag{4}$$

where x_i^d represents the ith agent's values in the dth dimension that bounded by the range $x_i^d \in \left(x_{min}^d, x_{max}^d\right)$.

b. Fitness value (*fit*) for each agent is calculated through Eq. (2) based on its solution values, which contain the coordinates and velocities. The best (minimum) fitness value fit_{best} and its solution X_{best} are recorded

c. fit_{best} is compared to the tolerance ε (stopping criteria) to decide whether to accept the solution or continue the iteration.

d. The calculation of the interacting force is written as

$$F_{ij}^d(k) = G(k)\frac{M_{pi}(k)\times M_{aj}(k)}{R_{ij}(k) + \lambda}\left(x_j^d(k) - x_i^d(k)\right), \tag{5}$$

where $F_{ij}^d(k)$ denotes the interaction force between agents j and i at the dth dimension in the kth step; $M_{pi}(k)$ and $M_{aj}(k)$ are the passive mass for agents i and active mass for agents j, respectively; and λ is set to be a small constant value to maintain the stability for small R_{ij}. $G(k)$ is the gravitational constant that evolving with the iteration time step k:

$$G(k) = G_0 e^{-\alpha\frac{k}{K}} \tag{6}$$

where the initial gravitational coefficient G_0 and gravitational attenuation coefficient α are constant coefficients based on the range of solution space at each dimension, K denotes the total number of the iteration step. $R_{ij}(k)$ is the Euclidian distance between the two agents:

$$R_{ij}(k) = \left\|X_i(k), X_j(k)\right\|_2. \tag{7}$$

The resultant force at the dth dimension for agent i can be written as

$$F_i^d(k) = \sum_{j=1, j\neq i}^{N} \text{rand}_j F_{ij}^d(k), \tag{8}$$

where $rand_j$ is a random value in the range of [0,1], which introduces the randomness into the searching progress to improve its ability for avoiding the local minimum value. The inertia mass M_i of an agent i is updated every iteration step according to its fitness values:

$$M_{ai} = M_{pi} = M_{ii} = M_i, \ (i = 1, 2, \ldots, N), \tag{9}$$

$$m_i(k) = \frac{fit_i(k) - worst(k)}{best(k) - worst(k)}, \tag{10}$$

$$M_i(k) = m_i(k) / \sum_{j=1}^{N} m_j(k), \tag{11}$$

where a better solution is guaranteed with a larger mass in the searching progress. For a minimum values problem, the best and worst is defined as:

$$\text{best}(k) = \min_{i\in\{1,2,\ldots N\}} fit_i(k), \tag{12}$$

$$\text{worst}(k) = \max_{i\in\{1,2,\ldots N\}} fit_i(k). \tag{13}$$

e. With a known resultant force and mass, the acceleration and velocity of each agent at dth dimension can be updated by

$$a_i^d(k) = \frac{F_i^d(k)}{M_i(k)}, \tag{14}$$

$$v_i^d(k+1) = rand_i \times v_i^d(k) + a_i^d(k). \tag{15}$$

f. At the end of an iteration step, the position of agents is updated with its velocity:

$$x_i^d(k+1) = x_i^d(k) + v_i^d(k+1). \tag{16}$$

g. After the update of positions, a new iteration step is initiated to calculate new fitness values; if error criteria are fulfilled or the maximum number of iterations has reached, the algorithm gives the result of MSL and the best fitness value. Figure 2 shows the framework of GSA–MSL that includes the procedures of data input and output.

The searching progress of GSA is visualized in a three-dimensional space. The initial gravitational coefficient $G_0 = 100$, gravitational attenuation coefficient $\alpha = 20$, the number of agents is 100, and total iteration steps are 1000. The initial position of agents is randomly given, and initial

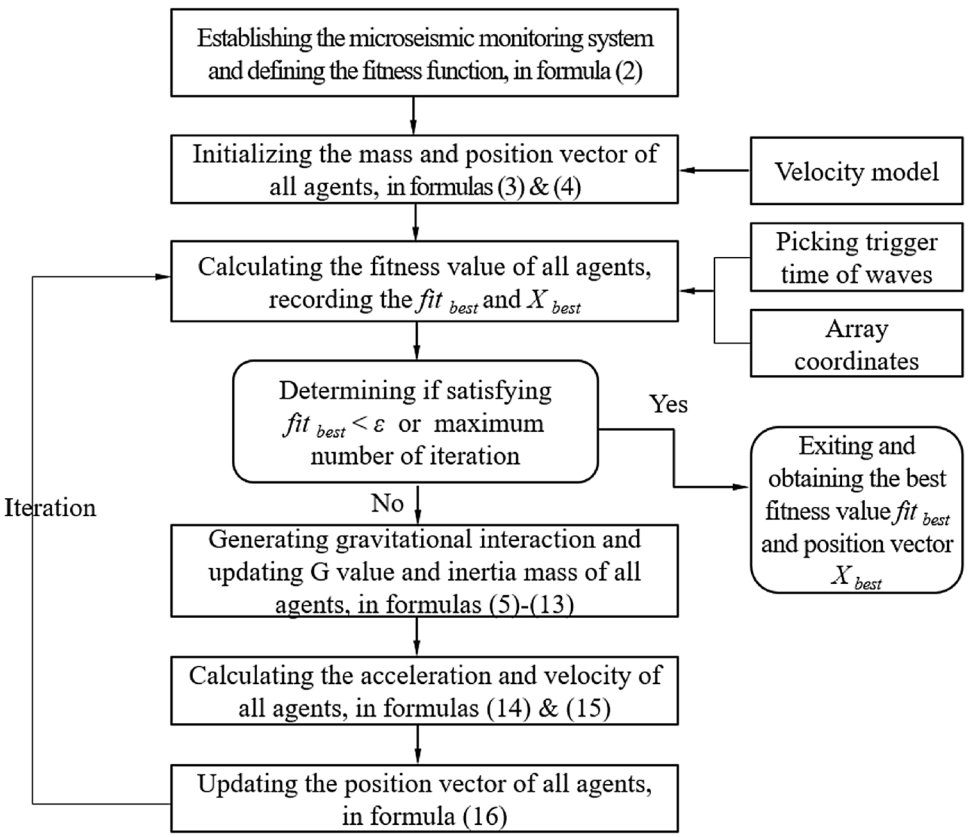

Fig. 2 Searching process of GSA–MSL

values of mass are 0.5. The size of an agent represents its mass that linked with its fitness value at the current step (Fig. 3a). Gravity forces are generated between agents; larger mass agents (high-quality solutions) apply stronger attractive forces to small agents at each iteration step. The position, fitness values, and mass (Fig. 3b, c) are constantly updated. As iteration goes on, the agents are attracted by each other and converging towards the global optimal solution (Fig. 3c). Eventually, all agents are converged to the global optimal solution, as shown in Fig. 3d.

2.3 Advantages and Limitations of GSA–MSL

As a heuristic algorithm, GSA possesses unique advantages over classic MSL methods, which can be categorized as iterative and non-iterative methods. Non-iterative methods (e.g., USBM, Inglada) are favored for their simple implementation. However, the most common problem for these methods is the assumption of a single velocity in the underground space, which severely restricts their application for tunnel engineering (Ge 2003a, b). Iterative MSL methods (e.g., Geiger's Method and Thurber's Method) could avoid such issue by building a series of arrival-time functions and thus more suitable for the multi-velocity situation. However, their convergence highly relies on the quality of the initial solution. This is because the Tylor expansion is necessary for the linearization of the arrival-time function. Based on this linearization, the Jacobian or Hessian matrix is calculated as the coefficient matrix. Therefore, the convergence of the iterative methods cannot be guaranteed (Ge 2003a, b), and it is particularly true if a complicated velocity model is involved. The GSA–MSL could easily overcome both issues. It allows the consideration of a complex velocity model through the fitness function (Eq. 2), and it is much more robust for the quality of the initial values, since its initial agents are populated in the solution space.

Theoretically, GSA could be regarded as an advanced mutation of particle swarm optimization (PSO), since they are sharing a similar algorithm frame: a group of agents is updated towards the optimal one at each iterative step in a pre-defined solution space, and eventually converges to the global optimal solution. However, there are two main

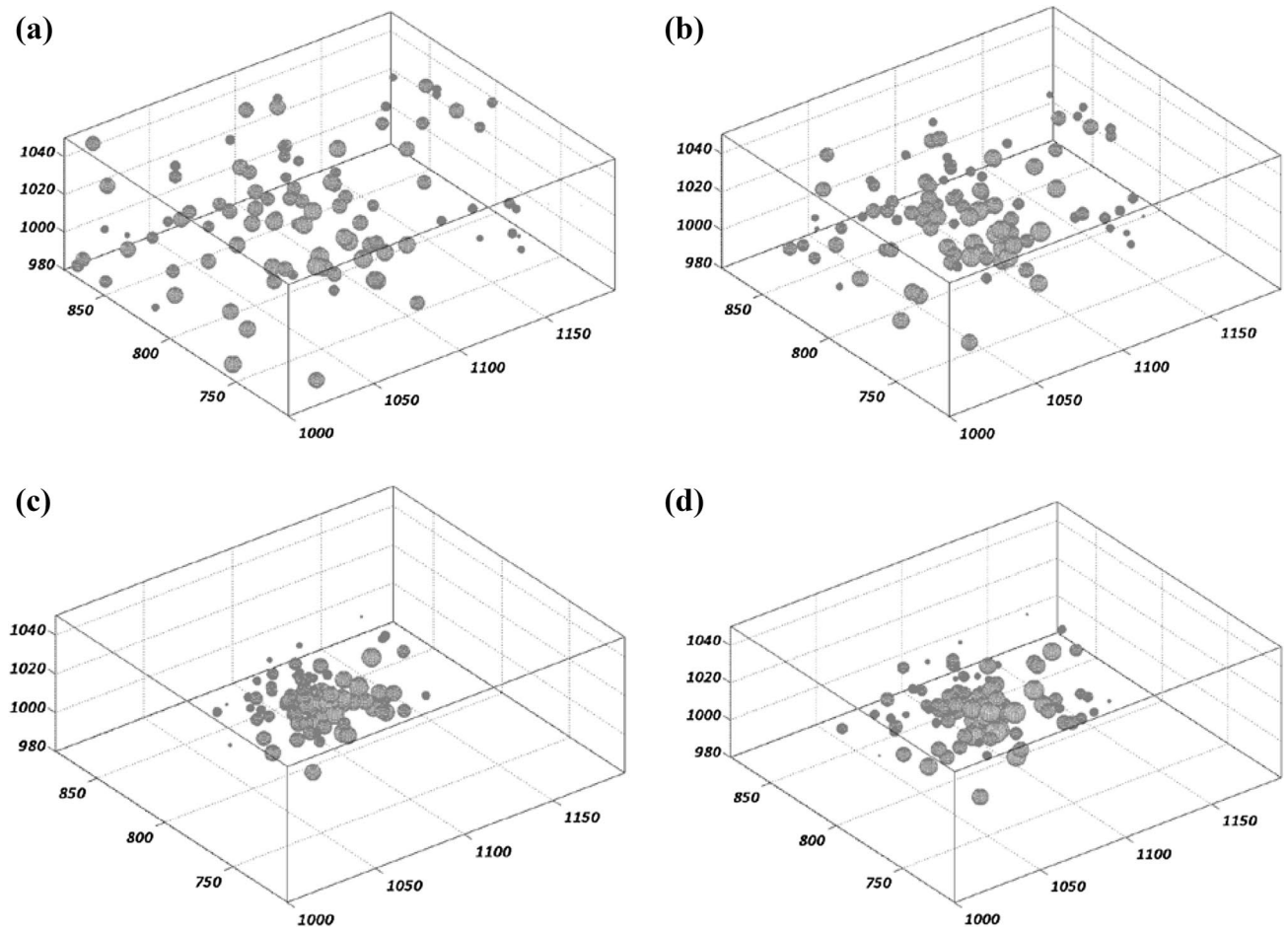

Fig. 3 The movement of agents in the solution space during the GSA searching process. **a** Initial; **b** and, **c** in progress; **d** final positions

attributes that make the GSA far more accurate and efficient. First, due to the gravitational equation, the attractive forces are ubiquitous in the solution space, which allows all the agents to participate in the updating process and thus provides GSA a higher speed of convergence. It also grants a better ability for GSA to avoid the local optimal solution. The updating strategy of PSO only involves the individual and global best fitness value (i_{best} and g_{best}). Second, GSA does not require the storage of i_{best} and the comparison between i_{best} and g_{best}, while PSO does. Apparently, with a large number of agents or iteration steps, these extra procedures would make PSO more computationally expensive.

The GSA–MSL inevitably suffers the common limitations existing in the family of the heuristic algorithm. Despite its optimal performance, GSA cannot provide an analytical formula for estimating the speed of convergence or accuracy. Neither can we quantitatively analysis its sensitivity for the parameters such as the value of the gravitational attenuation constant (Eq. 6). The convergence cannot be guaranteed if the dimension of the solution space is as high as seven or eight, while the formation of the sensor array is limited in the tunnel space. Unexpected errors could also be introduced by the poor quality of the MS singles. Still, the tests that conducted with both synthetic and real data demonstrate the superior performance of GSA–MSL. It indicates that this method is more stable and accurate than its competitors and predecessors.

3 Performance Analyses of Microseismic Source Location

In this section, the accuracy and computational efficiency of GSA–MSL are first tested with synthetic microseismic data generated by a simplified model, and then, it is further applied with real data collected from a twin-tube tunnel. The particle swarm optimization algorithm (PSO) and another non-heuristic-algorithm simplex algorithm (SA) are used as comparisons to demonstrate the ability of GSA for searching the global optimal value with optimal efficiency. Both PSO and GSA use 1000 agents with a random initial distribution for all the tests.

3.1 Performance Analyses by Synthetic Microseismic Data

Five synthetic microseismic data sets are generated to study the performance of the algorithms in the simplest situation. This model is simplified as a full-infinite space with a homogeneous velocity; no influence of tunnel space or geological structure is involved. Therefore, a four-dimensional solution space is constructed with three position coordinates and one velocity value. A fixed sensor array with nine sensors well covers all the microseismic sources, which means no limitation applied to the layout of the sensor array. Since these assumptions of synthetic model guarantee the convergences of all three methods, the performances will be able to reflect the fundamental difference of these algorithms. Conditions of source coordinates, velocity, and arrival time are listed in Table 1 (the trigger time is $t=0$).

The searching process of the solution (source location and velocity) and the changes of fitness value are shown in Fig. 4. The number of convergence step, minimum fitness value, and location error is used to evaluate the performances. All the final solutions, from an engineering perspective, can be regarded as accurate MSL due to the simplification of the model. However, there are few important features must be noticed. SA, as a non-heuristic algorithm, has relatively the worst performance; both speed of convergence and search accuracy are much lower than those of the other two. For the comparison between the heuristic algorithms, GSA does not always provide better accuracy than that of PSO. Such result is also caused by the idealized assumptions. However, as discussed earlier, GSA shows a distinctively higher speed of convergence. The results of the synthetic data tests support the theoretical analysis of GSA's better performance.

3.2 Performance Analyses in the Twin-Tube Tunnel Engineering

3.2.1 Microseismic array and velocity models in the tunnel

To better demonstrate the optimal performance of GSA–MSL more complicated models needs to be used. The GSA–MSL is applied for the twin-tube tunnel engineering, which usually accompanied by abundant MS events during its excavation. An MS-monitoring system and the layout of the sensor array are shown in Fig. 5. Both tunnels are monitored sectionally with three sensors as one group; two sensor groups (*L1* and *L2*) are distributed at the leading tunnel and one (*F3*) at the following tunnel; three sensors in each group are located at the top and two sides of the tunnel, respectively. The sensor group at the leading tunnel has the effect of covering the monitoring range of the following tunnel and improves the accuracy of the MSL in that range. The data acquisition station is installed at the lining support area, which is in a crossing tunnel between two tubes.

As discussed earlier, the heuristic-algorithm-based MSL has an advantage for searching the optimal solution in a high-dimensional solution space and, therefore, allows the use of a more realistic velocity model. Here, we propose four types of wave velocity model for MSL in deep-buried tunneling based on the common orientations of underground strata. The influence of tunnel's excavated area for MS singles is also considered.

Table 1 PSO, GSA, and SA methods for MSL based on the synthetic data set

	Calculation conditions		
	Coordinates of synthetic source	Velocity (m/s)	Arrival time of microseismic sensor array (E−3s)
Case 1	(50, 30, 0)	5000.0	9.4, 7.8, 8.4, 9.1, 7.8, 8.7, 5.9, 6.1, 6.3
Case 2	(45, 30, 0)	5100.0	8.5, 6.9, 7.6, 9.6, 8.4, 9.2, 6.7, 6.9, 7.1
Case 3	(50, 35, 0)	5200.0	9.7, 8.2, 8.8, 9.5, 8.2, 9.0, 5.9, 5.8, 6.1
Case 4	(50, 30, 5)	5300.0	8.9, 7.4, 7.9, 8.6, 7.4, 8.1, 5.6, 5.8, 5.8
Case 5	(45, 35, 5)	5400.0	8.9, 7.3, 7.9, 9.8, 8.6, 9.3, 6.6, 6.5, 6.7

Search result and error analyses

Methods	GSA			PSO			SA		
Indicators	(1)/steps	(2)	(3)/m	(1)/steps	(2)	(3)/m	(1)/steps	(2)	(3)/m
Case 1	6	7.3E−6	0.58	21	8.4E−6	0.43	60	2.3E−4	3.21
Case 2	9	2.4E−5	0.90	50	1.5E−5	0.95	65	4.2E−4	2.09
Case 3	4	1.8E−5	1.70	24	1.5E−5	1.74	55	2.7E−4	4.16
Case 4	7	2.7E−5	0.94	20	9.7E−6	0.66	78	5.9E−4	5.48
Case 5	3	3.0E−5	1.47	60	1.2E−5	1.71	94	6.1E−4	5.63

Indicator (1) denotes the convergence steps; (2) denotes the minimum fitness value; (3) denotes the absolute values of the location error

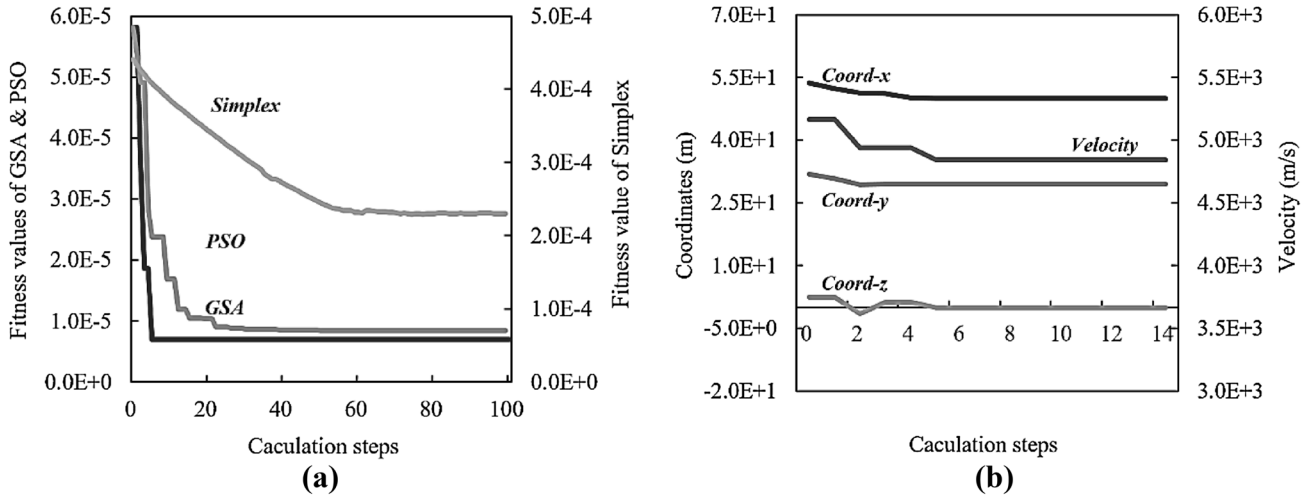

Fig. 4 Search process for optimal fitness value and solution in Case 1. **a** Searching for the optimal fitness value by the three methods, **b** searching for the solution by the GSA method

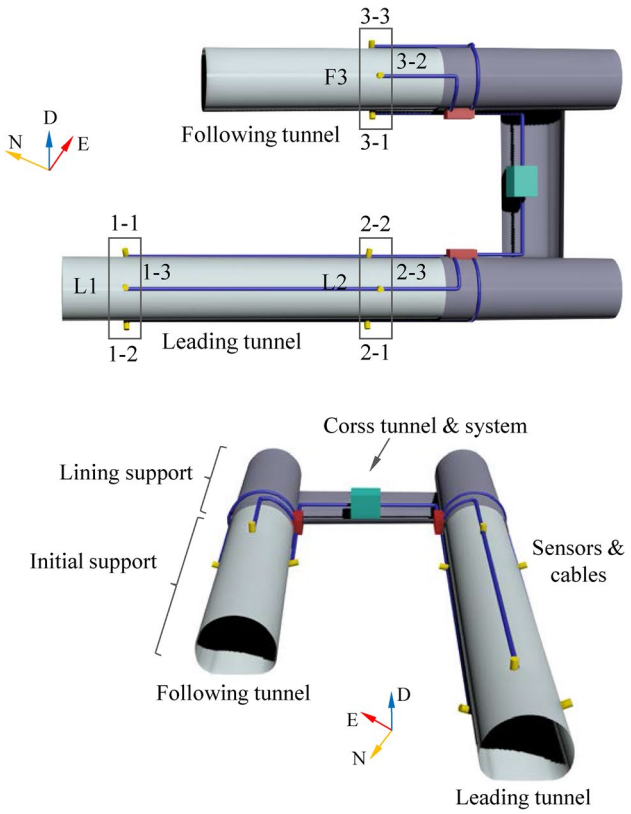

Fig. 5 MS-monitoring system and layout of the sensor array in a twin-tube tunnel. **a** Model I, **b** Model II, **c** Model III

(i) Model I (Fig. 6a) is the sectional velocity model or triple-velocity group. It means that the equivalent velocity at each sensor group is unique and should be considered as different values for the MSL algorithm. This model is proposed to represent the heterogeneity of geological conditions, which is strong along the tunnel but negligible at the same section. This model is particularly useful when the orientation of strata and the tunnel are nearly perpendicular to each other.

(ii) Model II (Fig. 6b) divides the sensors into different velocity groups based on their specific locations. There are two situations that are suitable for using model II: one is when the heterogeneity of strata is strong both along the tunnel and at the same section. Therefore, sensors should be divided into three velocity groups according to their regional lithology: group 1 (1–2, 1–3), group 2 (1–1, 2–1, 2–2, and 2–3), and group 3 (3–1, 3–2, 3–3). The other situation is when the stress-induced seismic anisotropy needs to be considered. In which case, seismic signals that propagate along the direction of the maximum principal stress have the highest velocity. Sensors should also be categorized based on their local stress state.

(iii) Model III (Fig. 6c) divides the sensors into different velocity groups based on their relative position to microseismic sources. It is proposed to represent the influence of the void space of the tunnel. The propagation of microseismic signal might be strongly affected if its wavelength is on the same scale of the length of the tunnel's cross section. For example, sensors 1–2 and 2–1 at the leading tunnel may receive a distorted MS signal triggered at the black dot. Because the void space of the leading tunnel could significantly delay the signal. If such phenomenon is found, they should be assigned with the same velocity value, which is different from unaffected sensors (1–1, 1–3, 2–1, 2–3) and the sensor group *F3* at the following tunnel.

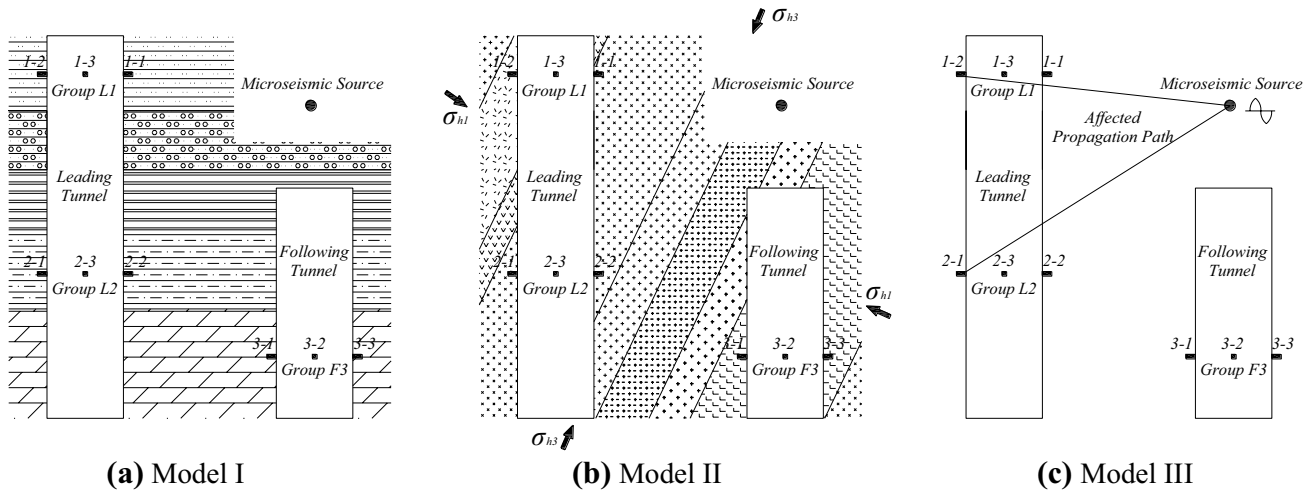

Fig. 6 Schematic diagram of wave velocity model of tunnel surrounding rock

(iv) (iv) If both geological heterogeneity and the effect of void space need to be considered, the Model IV should be to be used. It is a combination of model I or II and model III. In this case, more variables of velocity need to be introduced into the algorithm and the solution space would have an even higher dimension.

3.2.2 Five-dimensional searching test in the tunnel

The accuracy and computational efficiency of GSA are tested in this section with real microseismic data and velocity models proposed in the previous section. Similarly, the PSO and SA algorithms are used as comparisons to demonstrate the ability of GSA for searching the global optimal value in various situations. Equation (2) is also applied here as the fitness function for all the tests and algorithms. The trigger time, velocity model, and coordinates of sensors for each test are detailed in Table 2 and calculation results are shown in Table 3.

The five-dimensional test searches a solution space with three-dimensional source coordinates and two equivalent velocities. The actual source location in Case 6 is 908, 900, and 1020 m. It is located near the following tunnel. The velocity model III is used to construct the solution space, which includes three unknown source coordinates plus $V1$ for void-unaffected sensors (1–1, 2–2, 2–3) and $V2$ for void-affected sensors (1–2, 2–1). According to the searching results, GSA provides a minimum absolute error (5.995 m) that slightly better compared with that of PSO (6.5 m). SA fails to provide a reasonable result as its error reaches to 36.8 m due to its poor ability to avoid local minimum values in a solution space with multiple variables. Both heuristic methods are reliable enough for the engineering requirement.

The convergence progress for each algorithm is shown in Fig. 7. It can be observed from the figure that GSA has the highest speed of convergence. Its exceptional capacity for the 'communication' enables all the agents in GSA to converge towards the global optimal solution within six iterations. PSO needs more than 300 steps to converge. The irregular shape of its iteration curve indicates the searching progress in not uniformly converging towards the final solution. Such lower speed also results from its deficiency in 'communication'. SA has the slowest progress and eventually stopped at a position with the lowest accuracy.

3.2.3 Six-Dimensional Searching Test in the Tunnel

This test involves using Case 7 (model III) and Case 8 (mode I). The searching process is shown in Figs. 8 and 9, respectively. Both cases have three velocities which together with the coordinates construct a six-dimensional solution space. Similarly, the GSA has the best performance in both accuracy and efficiency; the source is located with a percentage error of 8.9–14.9% for Cases 7 and 8, respectively. These high-accuracy results are obtained within ten iterations. PSO can locate the source position with acceptable accuracy, and its convergence is completed within 150 steps. SA cannot provide a reliable solution and shows a non-converging performance.

In addition to the above three test cases, Table 4 listed performances of Cases 9, 10 with velocity model III and Cases 11, 12 with velocity model I. Like the Cases 6–8, GSA received a reliable result within a range of 5–23 steps, while the searching process of PSO converges in a range of

Table 2 Trigger time, velocity model, and coordinates of the sensor array

Sensor array		Sensor group *L1*			Sensor group *L2*			Sensor group *F3*		
		1–1	1–2	1–3	2–1	2–2	2–3	3–1	3–2	3–3
Array 1	North (m)	868.37	861.8	–	835.38	841.91	845.61	860.14	862.84	866.82
	East (m)	847.29	832.15	–	846.47	860.16	852.13	889.99	895.12	904.63
	Depth (m)	1007.9	1007.9	–	1008.4	1008.6	1016.6	1009.6	1017.3	1009.7
Case 6	Trigger time (s)	0.4938	0.5002	–	0.5012	0.4973	0.4973	–	–	–
	Velocity model	*V*1	*V*2	–	*V*2	*V*1		–	–	–
Case 7	Trigger time(s)	0.4988	0.5027	–	0.5051	0.5002	0.5003	0.4907	0.4904	0.4882
	Velocity model	*V*1	*V*2	–	*V*2	*V*1		*V*3		
Sensor array		Sensor group 1#			Sensor group 2#			Sensor group 3#		
		1–1	1–2	1–3	2–1	2–2	2–3	3–1	3–2	3–3
Array 2	North (m)	936.19	931.73	932.14	901.93	908.86	904.35	893.46	896.87	901.89
	East (m)	814.92	798.12	805.86	811.06	827.74	818.91	873.96	877.95	886.39
	Depth (m)	1007.9	1007.2	1015.4	1007.1	1007.3	1015.4	1010.7	1017.9	1010.8
Case 8	Trigger time(s)	0.496	0.4964	0.4967	0.5007	0.5021	0.5019	0.5177	0.5186	0.5024
	Velocity model	*V1*			*V2*			*V3*		

Two sensor arrays with different three-dimensional coordinates (north, east, and depth) are selected for MSL; Case 1 and Case 2 (microseismic sources) are collected from array one and Case 3 collected from array two; equivalent velocities (*V*1, *V*2, and *V*3) are assigned to sensors; "–" indicates that the sensor was not deployed or selected for a searching process of MSL

Table 3 PSO, GSA, and Simplex-based source location method (search results and error analysis)

		Search results								
Case 6	Methods	North (m)	East (m)	Depth (m)	*V*1 (m/s)			*V*2 (m/s)		
	GSA	911.2	904.4	1017.4	5768.47			5185.25		
	PSO	905.8	894.2	1021.9	5523.11			5000.02		
	SA	930.5	928.8	1015.1	5424.62			5241.22		
Case 7	Methods	North (m)	East (m)	Depth (m)	*V*1 (m/s)	*V2* (m/s)				*V3* (m/s)
	GSA	916.4	919.8	1006.9	4231.55	4106.49				4856.42
	PSO	912.2	911.2	1002.6	3736.25	3567.57				4103.88
	SA	936.5	931.0	1006.7	4758.6	4613.61				5077.58
Case 8	Methods	North (m)	East (m)	Depth (m)	*V*1 (m/s)	*V*2 (m/s)				*V*3 (m/s)
	GSA	1014.4	766.4	1012.1	5566.37	5600.91				4178.35
	PSO	1001.6	792.8	999.1	5856.71	5936.65				4085.45
	SA	972.3	807.6	1014.6	5008.08	5020.23				4988.02
	Actual source location				Error analysis					
	North (m)	East (m)	Depth (m)		GSA (m & %)		PSO (m & %)		SA (m & %)	
Case 6	908	900	1020		5.995	12.2	6.5	13.2	36.824	74.6
Case 7	910	920	1010		7.105	14.9	11.717	24.5	28.911	60.6
Case 8	1008	770	1010		7.648	8.9	26.074	30.4	52.065	60.7

60–293 steps. SA still shows a poor performance of speed of convergence or fails to provide an acceptable result.

4 Engineering Case Study

A representative rockburst hazard is chosen to demonstrate the ability of GSA for guiding the early warning of the rockburst and interpretation of unstable areas. This

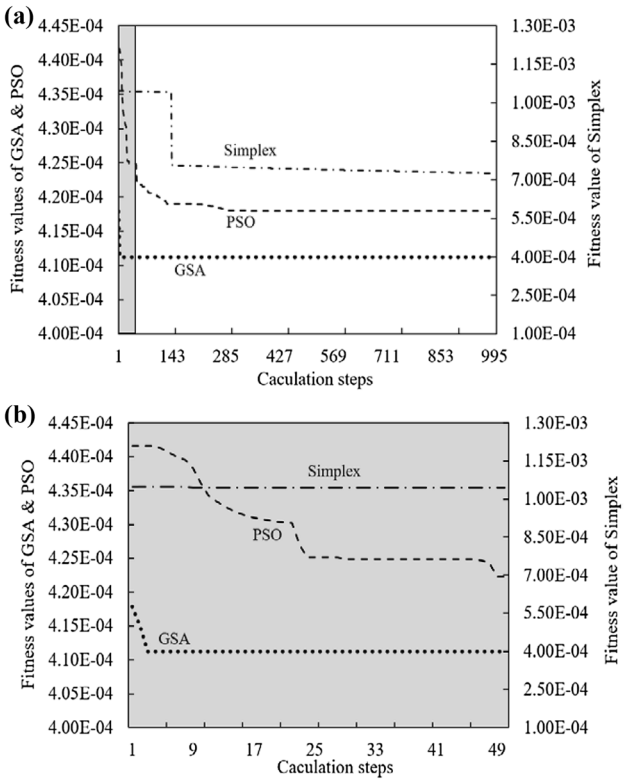

Fig. 7 Search process for fitness values of GSA, PSO, and simplex optimal agent in Case 6. **a** Entire search process in 1000 steps, **b** enlarged grey area for first 50 steps

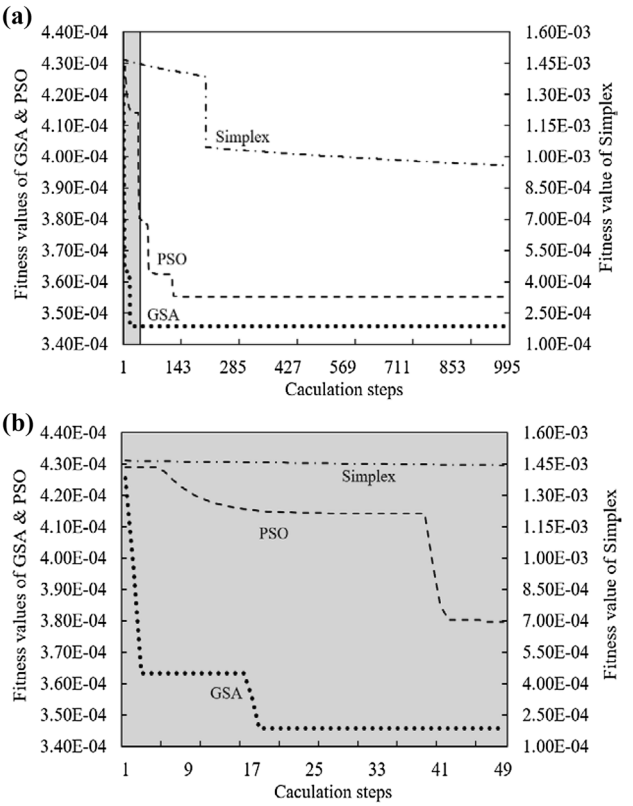

Fig. 8 Search process for fitness values of GSA, PSO, and simplex optimal sample in Case 7. **a** Entire search process in 1000 steps, **b** enlarged grey area

accident was accompanied by a serial of microseismic events which released during a brewing time of the rockburst. The locations of these events form a cluster, which could informatively indicate the unstable area around the tunnel. The correctness of this indication mainly depends on the accuracy of MSL. Meanwhile, if the MSL has a proper efficiency, an immediate MS monitoring can be achieved. By combining the accurate MSL information and temporal distribution of the MS events, an effective early warning framework for the rockburst can be built. It could prevent the casualty and economic losses during tunneling.

4.1 Engineering Overview

The microseismic monitoring tests were conducted at the high-risk area of Michang mountain twin-tube tunnel in China. It spans Sichuan and Shanxi province with a total length of 13.8 km, which is ranked as the third longest highway tunnel in the world. Its geographical position is shown in Fig. 10a.

Strong rockburst events were repeatedly observed at the area of K45 + 880–K46 + 170 due to the local high stress in the surrounding rock strata. The depth of this area ranges from 530 m to 760 m. The regional lithology mainly contains quartz diorite, gabbro, and tectonic granulite. The grade of surrounding rocks consists of grade III, and grade II with partially grade IV. Especially, the alternating layout of gabbro and tectonic granulite is the dominating pattern (Fig. 10b). It represents a tectonic granulite section, where rockburst hazards usually occur. The original rock of the tectonic granulite is granitic rock, which was broken down by the tectonic compression and later transformed into granular rock under the effect of static recrystallization. Such a phenomenon also indicates that micro-fractures in the rock mass were generated by a horizontal compressive force during the diagenetic process.

The features of rockburst are complicated due to the special geological conditions. The maximum energy of microseismic events from the rockburst can reach millions of joules. It even equals the energy that required for tunnel drilling and blasting activity. Under the impact of large-energy microseismic events, construction equipment in the tunnel was overturned, the surrounding rocks (sidewall and floor) show a large area of cracking, dislocation, and collapse and supports structures of the tunnel are severely damaged. The Rockburst zone is controlled by two or more

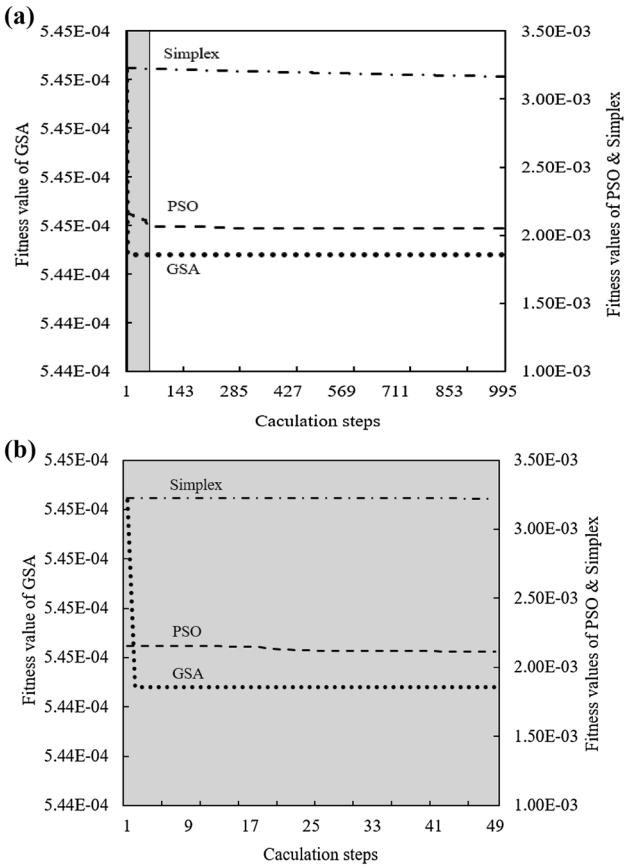

Fig. 9 Search process for fitness values of GSA, PSO, and simplex optimal sample in Case 8. **a** Entire search process in 1000 steps, **b** enlarged grey area

sets of fracture planes, and deposits left by the burst events are highly fragmented. There are several failure types of rockburst in the Micang Mountain tunnel, such as two-tube rockburst, tunnel roof or face rockburst, and hazard by large-energy shock, see Fig. 11.

The MS events that accompanied these rockbursts are recorded in both temporal and spatial scale with their moment magnitudes. It can be observed from Fig. 12a, b that multiple rockburst hazards are developed and a serial of MS signals are received during the brewing process of these rockburst events. Such phenomenon indicates a potential causality between MS events and rockbursts, which would allow us to use this information of MSL to achieve the early warning or prediction.

4.2 Application and Discussion

To better understand how to choose a proper velocity model in real field, we need to first look at two minor MS events that happened near the tunnel face of the leading and following tunnel, respectively. The layout of the sensor array is shown in Fig. 14 and their recorded signals are provided in Fig. 13. Figure 13a indicates that velocity model I is more suitable for the MSL of leading-tunnel event. Because the arrival time for each sensor group shows a clear spatial sequence of *L1*, *L2,* and *F3*, while the difference of arrival time within the same group is much smaller. Therefore, the sectional velocity model (Model I) is better for the MSL algorithm.

However, the same velocity model cannot be applied to the following tunnel event. It can be observed from Fig. 13b that there are strong differences of the arrival time between sensors within the same group (1–1, 1–2 and 2–1, 2–2). The differences for *L1* (1–1, 1–2) and *L2* (2–1, 2–2) are 4.4E−3 and 3.4E−3, respectively, which exceed the theoretical limit of the arrival-time difference that made based the single-velocity assumption. This is because the MS signal released from the following tunnel event is significantly delayed by the void part of the leading tunnel. The seismic wave reached the leading tunnel and propagates along its surface in a velocity that closes to the Rayleigh wave. Hence, the velocity model (Model III) that considers this effect should be used for the MSL.

A distinctive rockburst hazard and its pre-burst MS events that occurred at the following tunnel in 12.29.2017

Table 4 Convergence steps and minimum fitness value for all test cases

Methods	GSA		PSO		SA	
Results	Convergence steps	Minimum fitness value	Convergence steps	Minimum fitness value	Convergence steps	Minimum fitness value
Case 6	5	0.00041	293	0.00042	–	0.00073
Case 7	18	0.00035	140	0.00036	–	0.00096
Case 8	4	0.00054	68	0.00205	–	0.00317
Case 9	5	0.00027	130	0.00027	703	0.00038
Case 10	11	0.00032	116	0.00032	742	0.00086
Case 11	8	0.00069	60	0.00059	–	0.00158
Case 12	23	0.00045	57	0.00071	512	0.00101

Italics are tested cases shown with the search process and results; "–" indicates convergence not achieved at the maximum number of iteration steps

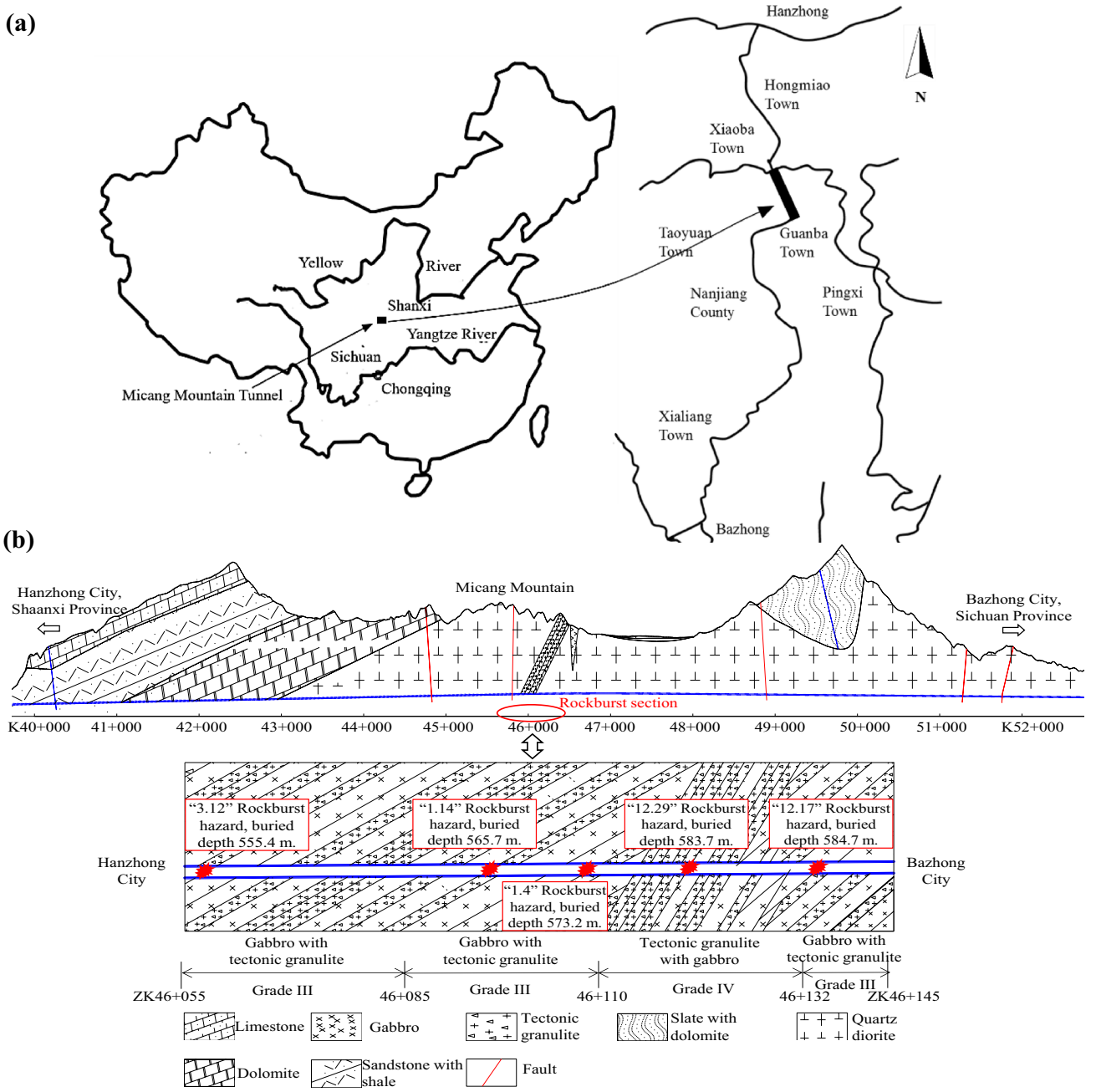

Fig. 10 Micang Mountain tunnel, China. **a** Location and plan of the Micang Mountain tunnel, **b** geological cross section along the tunnel

are chosen to further discuss the application of GSA–MSL for the rockburst. This event is brewed near the top of the following tunnel face. The local lithology and sensor layout are shown in Fig. 14.

The MS clusters obtained from the GSA–MSL are shown in Fig. 15. MSL results using both Model I and Model III are compared to determine the optimal velocity model. It can be observed from the figures that Model III obtains a better result. MS events are concentrated around the right wall area of the following tunnel, which is consistent with the actual locations; the results based on Model I is much less reliable, as the located events are sparsely distributed along the following tunnel with a relatively larger distance from each other. Such a result cannot precisely represent the unstable area that generates rockburst. The choose of the velocity model is crucial for the accuracy of the GSA or other MSL algorithms.

The magnitude of spatial deviations in Fig. 15 is further quantitatively evaluated. The distances between each seismic event and the averaged centre of the event cloud (i.e.,

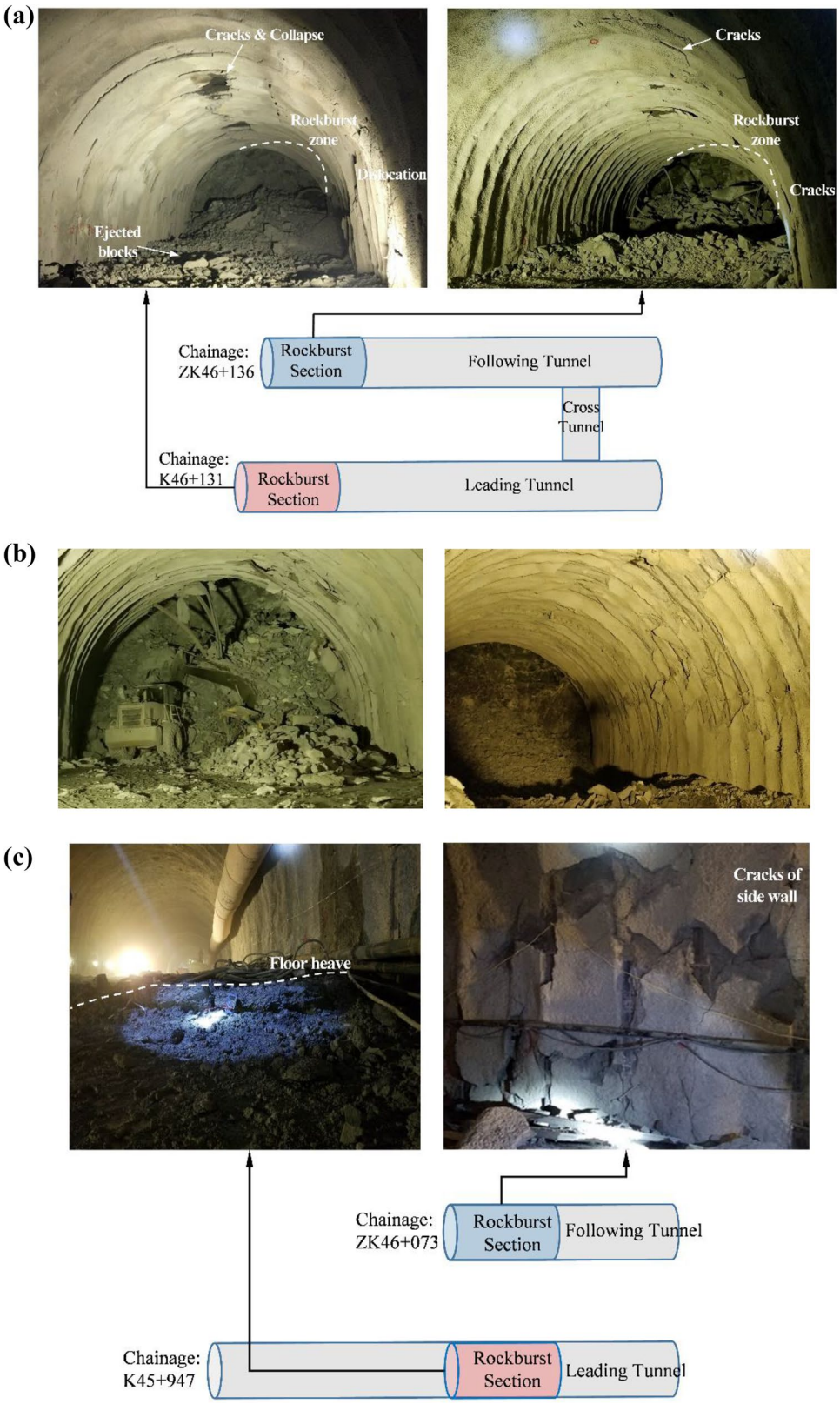

Fig. 11 Rockburst events in the Micang Mountain tunnel. **a** Two-tube rockburst on 17 December 2017, **b** tunnel roof and face rockbursts, and **c** hazard by large-energy shock on 2 March 2018

inter-event distance) are calculated. Then, the distribution of the percentage of events with different deviating magnitudes is shown in Fig. 16. The results indicate that for the reliable velocity model (Model III), the deviation distance distributed in a range of 1–61 m with the highest number of the event is at 20 m, which occupies 2.4%. The distribution

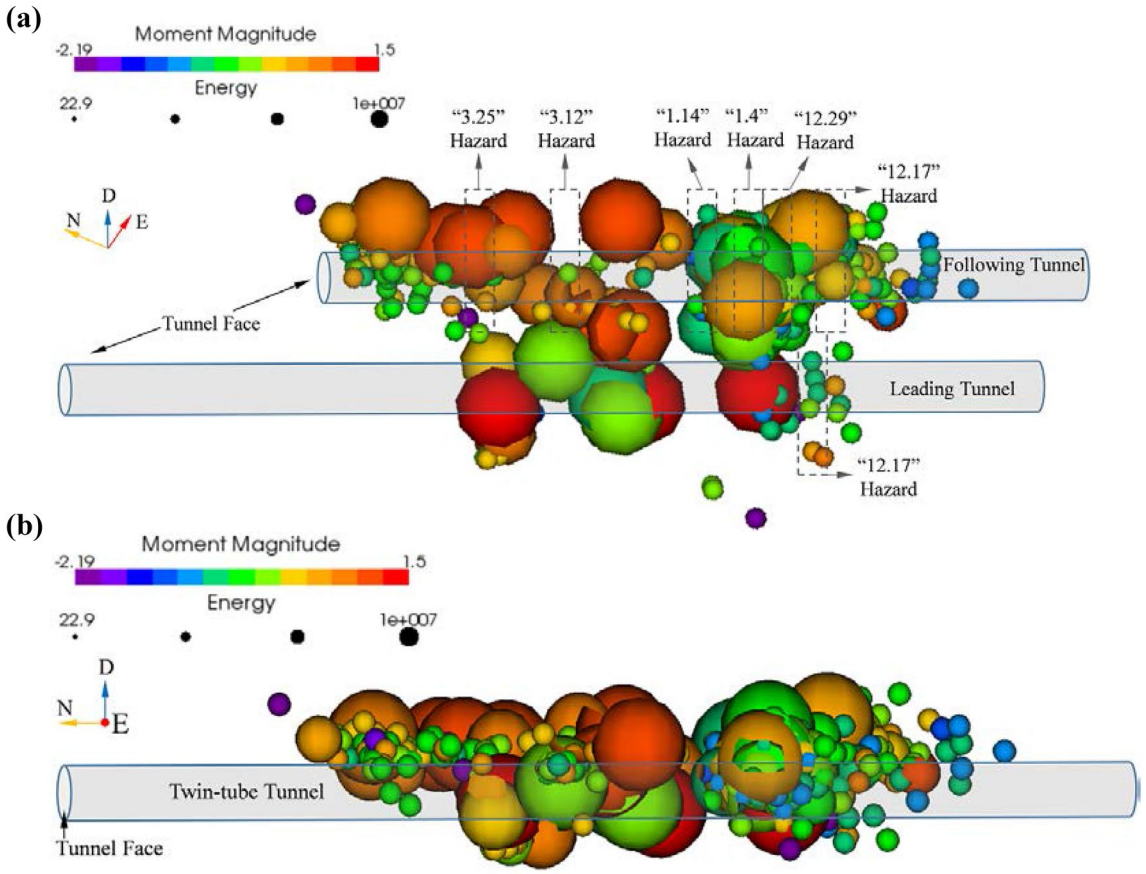

Fig. 12 Microseismic events' distribution along tunnels. **a** Plain view, **b** lateral view

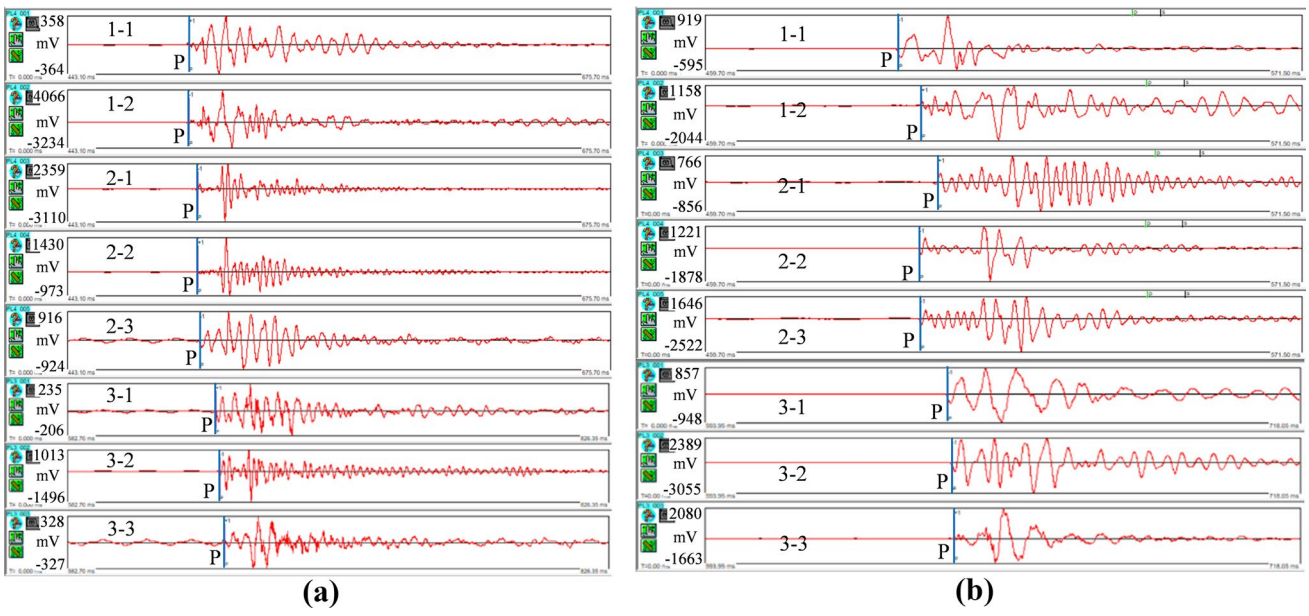

Fig. 13 **a** MS signals received from an MS event near the leading-tunnel face. **b** MS signals received from an MS event near the following tunnel face

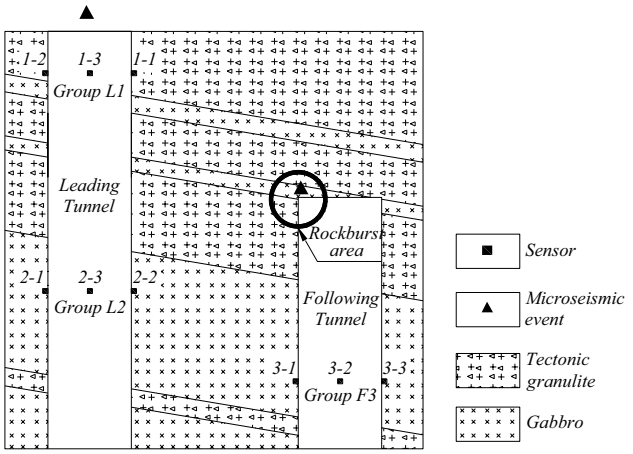

Fig. 14 Lithology and sensor layout along tunnel. The black circle denotes the area of "12.29" rockburst hazard; two black triangular dotes represent the two minor MS events at the leading and following tunnel, respectively

of inter-event distances is flattened towards a larger range in the unreliable model (Model I), which decreases the percentage of events with small deviations. These results suggest that the locations of MS events are relatively spread. Such results are less help for locating the unstable areas around the tunnel.

The performance of PSO and GSA is also further examined with the same set of data from other rockburst events. Figure 17 represents the percentage errors of MSL results in a different combination of algorithms (GSA and PSO) and velocity models (Model I and Model III). In general, the GSA has a higher accuracy for the same velocity model. This indicates the superior stability of the algorithm; the GSA is less affected by changes in the number of dimensions. In this case, the Model III shows better accuracy than that of Model I. It is mainly because the propagation of the seismic wave is affected by the void space of the tunnel. It must be pointed out that there is no velocity model that can be well applied to any case. The performance of a velocity model always depends on the actual geological conditions, which requires further information from the geological survey and analysis for the pattern of the arrival time.

5 Conclusions

An advanced heuristic algorithm is introduced for searching the location of microseismic events in the tunneling. Its framework is built with a twin-tube-tunnel MS-monitoring system. Four equivalent velocity models are proposed and further applied to the algorithms to demonstrate the performance of GSA–MSL. Using both synthetic and filed data, the accuracy and speed of convergence of GSA–MSL are rigorously examined and compared with heuristic and non-heuristic algorithms. It can be concluded from these studies that GSA is superior in both accuracy and speed of convergence than that of PSO for each velocity mode. The stability of GSA–MSL is outstanding, as its overall performance does not show a strong dependency upon the number of dimensions of the solution space. The variation of solutions also becomes negligible after the iteration reached a stable state. The non-heuristic algorithm, simplex algorithm, fails to provide reliable results, since it is not suitable for searching high-dimensional issues.

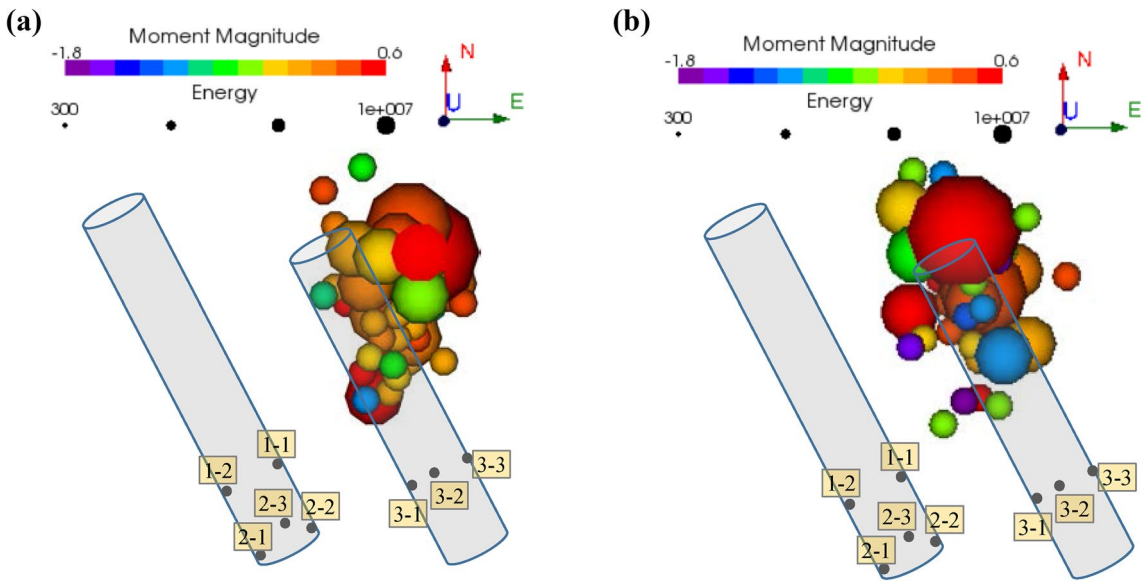

Fig. 15 Microseismic events location of "12.29" rockburst. **a** Velocity model III, **b** velocity model I

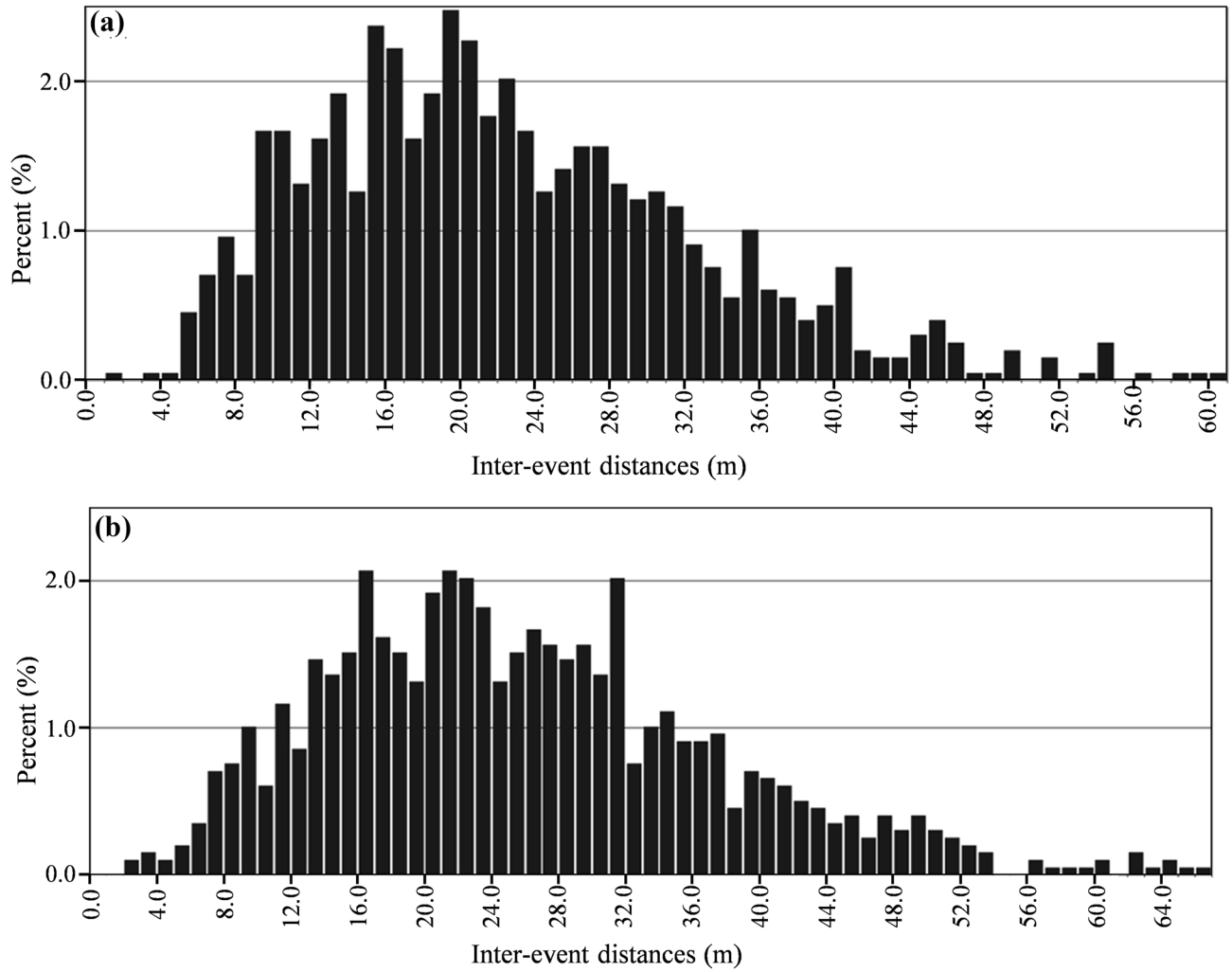

Fig. 16 Inter-event distance distribution of "12.29" rockburst. **a** Velocity model III, **b** velocity model I

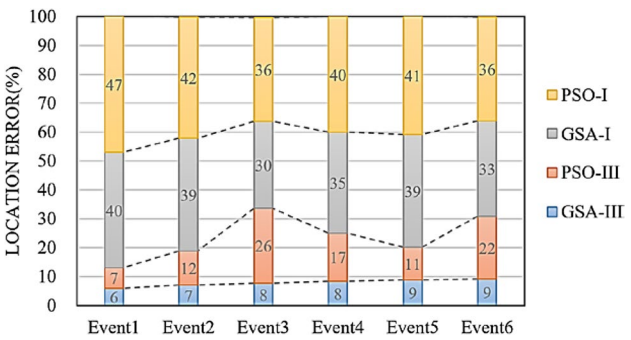

Fig. 17 Composition of location error in typical microseismic events

A representative case study prior to a strong rockburst event in the twin-tube tunnel is conducted using GSA–MSL. The results prove that GSA–MSL could accurately narrow the spatial distribution of clouds of MS events and help to further identify high-risk areas. It also indicates that velocity models presented in this paper could sufficiently cover typical situations, which include the heterogeneity of underground media and the effect of void space. A velocity model that properly considers the geological conditions could significantly reduce the searching errors and increase the speed of convergence. In conclusion, the computational advantages of GSA well satisfy the requirement of using realistic velocity model (i.e., more unknown quantities of velocities) in MSL. Optimal locating results can be obtained with a proper combination of GSA–MSL and velocity models. The gravitational searching algorithm shows a great potential to benefit the early warning of rock mass hazards in tunneling.

Acknowledgements This work was financially supported by the National Natural Science Foundation of China (Grant numbers 41807255 and 41772329); State Key Laboratory of Geohazard Prevention and Geo-environment Protection Independent Research Project (Grant number SKLGP2018Z016); Sichuan Science and Technology

Project (Grant number 2019YJ0465). The authors would also like to give special thanks to the engineers and project managers of Micang Mountain who collected the valuable data of rockburst in a high-risk environment. This study could not be completed without their unwavering professionalism.

References

Chen BR, Feng XT, Li SL, Yuan JP, Xu SH (2009) Microselsm source location with hierarchical strategy based on particle swarm optimization. Cn J Rock Mech Eng 28(4):740–749

Dorigo M, Member I, Maniezzo V, Colorni A (1996) Ant System: optimization by a colony of cooperating agents. IEEE Trans Syst Man Cybern B Cybern 26(1):29–41

Farmer JD, Packard NH, Perelson AS (1986) The immune system, adaption, and machine learning. Physica 22D:187–204

Feng GL, Feng XT, Chen BR, Xiao YX, Jiang Q (2015) Sectional velocity model for microseismic source location in tunnels. Tunn Undergr Space Technol 45:73–83

Feng XT, Chen BR, Ming HJ, Wu XY, Xiao YX, Feng GG, Zhou H, Qiu SL (2013) Evolution law and mechanism of rockbursts in deep tunnels: immediate rockburst. Cn J Rock Mech Eng 31(3):433–444

Gazi V, Passino KM (2004) Stability analysis of social foraging swarms. IEEE Trans Syst Man Cybern B Cybern 34(1):539–557

Ge MC (2003a) Analysis of soruce location algorithms part I: overview and non-iterative methods. J Acoustic Emission 21:14–28

Ge MC (2003b) Analysis of soruce location algorithms Part II: iterative methods. J Acoustic Emission 21:29–51

Gong SY, Dou LM, Ma XP, He J, Liu YG (2011) Study on the improvement of the microseismic network configuration for san He-Jian coal mine. Proc Eng 26:1398–1405

Gong SY, Dou LM, Ma XP, Mou ZL, Lu CP (2012) Optimization algorithm of network configuration for improving location accuracy of microseism in coal mine. Chin J Rock Mech Eng 31(1):8–17

Grigoli F, Cesca S, Vassallo M, Dahm T (2013) Automated seismic event location by travel-time stacking: an application to mining induced seismicity. Seismol Res Lett 84(4):666–677

Jiang Y, Xing HL (2016) Micro-seismic waveform matching inversion based on gravitational search algorithm and parallel computation (abstract). AGU fall meeting

Jones HR, Rayne CM (1994) The use of a genetic algorithm for the optimal design of microseismic monitoring networks. SPE/ISRM Rock Mech Petro Eng. Delft, The Netherlands: Society of Petroleum Engineers, pp 615–619

King A, Talebi S (2007) Anisotropy effects on microseismic event location. Pure Appl Geophys 164(11):2141–2156

Lagos SR, Velis DR (2018) Microseismic event location using global optimization algorithms: an integrated and automated workflow. J Appl Geophys 149:18–24

Li SJ, Liu YX, He X, Liu YJ (2003) Global search algorithm of minimum safety factor for slope stability analysis based on annealing simulation. Chin J of Rock Mech Eng 22(2):236–240

Li Y, Sui Q, Wang J, Wang Z, Jia L (2017). Localization of microseismic source based on Genetic-Simplex hybrid algorithm. In: Chinese Automation Congress, pp 4002–4007

Ma CC, Li TB, Xing HL, Zhang H, Wang MJ, Liu TY, Chen GQ, Chen ZQ (2016) Brittle rock modeling approach and its validation using excavation-induced micro-seismicity. Rock Mech Rock Eeng 49(8):3175–3188

Ma CC, Li TB, Zhang H, Wang JF (2018) An evaluation and early warning method for rockburst based on EMS microseismic source parameters. Rock Soil Mech 39(2):765–774

Pei D, Quirein JA, Cornish BE, Quinn D, Warpinski NR (2009) Velocity calibration for microseismic monitoring: a very fast simulated annealing (VFSA) approach for joint-objective optimization. Geophysics 74(6):47–55

Rashedi E, Nezamabadi-pour H, Saryazdi S (2009) GSA: a gravitational search algorithm. Inf Sci 179(13):2232–2248

Tang KS, Man KF, Kwong S, He Q (1996) Genetic algorithms and their application. IEEE Signal Process Mag 96:22–37

Vandenbergh F, Engelbrecht A (2006) A study of particle swarm optimization particle trajectories. Inf Sci 176(8):937–971

Wang J, Liu J, Liu H, Tian Z, Cheng F (2017) Modeling and locating underground water pipe leak with microseismic data. J Appl Geophys 136:1–8

Xiao YX, Feng XT, Hudson JA, Chen BR, Feng GL, Liu JP (2015) ISRM suggested method for in situ microseismic monitoring of the fracturing process in rock masses. Rock Mech Rock Eng 49(1):343–369

Yang Y, Wen J, Chen X (2015) Improvements on particle swarm optimization algorithm for velocity calibration in microseismic monitoring. Earthq Sci 28(4):263–273

Yuan D, Li A (2017) Joint inversion for effective anisotropic velocity model and event locations using S-wave splitting measurements from downhole microseismic data. Geophysics 82(3):133–143

Zhang J, Liu H, Zou Z, Huang Z (2015) Velocity modeling and inversion techniques for locating microseismic events in unconventional reservoirs. J Earth Sci 26(4):495–501